

# Tunable electronic and optical properties of monolayer silicane under tensile strain: A many-body study

Cite as: J. Chem. Phys. **141**, 064707 (2014); <https://doi.org/10.1063/1.4892110>

Submitted: 22 April 2014 . Accepted: 23 July 2014 . Published Online: 12 August 2014

Huabing Shu, Shudong Wang, Yunhai Li, Joanne Yip, and Jinlan Wang



View Online



Export Citation



CrossMark

## ARTICLES YOU MAY BE INTERESTED IN

[Hybrid functionals based on a screened Coulomb potential](#)

The Journal of Chemical Physics **118**, 8207 (2003); <https://doi.org/10.1063/1.1564060>

[Electronic properties of hydrogenated silicene and germanene](#)

Applied Physics Letters **98**, 223107 (2011); <https://doi.org/10.1063/1.3595682>

[Tunable gaps and enhanced mobilities in strain-engineered silicane](#)

Journal of Applied Physics **115**, 033711 (2014); <https://doi.org/10.1063/1.4860988>

Lock-in Amplifiers

Find out more today



Zurich  
Instruments

# Tunable electronic and optical properties of monolayer silicane under tensile strain: A many-body study

Huabing Shu,<sup>1</sup> Shudong Wang,<sup>1</sup> Yunhai Li,<sup>1</sup> Joanne Yip,<sup>2</sup> and Jinlan Wang<sup>1, a)</sup>

<sup>1</sup>Department of Physics & Key Laboratory of MEMS of Ministry of Education, Southeast University, Nanjing 211189, China

<sup>2</sup>Institute of Textiles and Clothing, The Hong Kong Polytechnic University, Kowloon, Hong Kong, China

(Received 22 April 2014; accepted 23 July 2014; published online 12 August 2014)

The electronic structure and optical response of silicane to strain are investigated by employing first-principles calculations based on many-body perturbation theory. The bandgap can be efficiently engineered in a broad range and an indirect to direct bandgap transition is observed under a strain of 2.74%; the semiconducting silicane can even be turned into a metal under a very large strain. The transitions derive from the persistent downward shift of the lowest conduction band at the  $\Gamma$ -point upon an increasing strain. The quasi-particle bandgaps of silicane are sizable due to the weak dielectric screening and the low dimension; they are rapidly reduced as strain increases while the exciton bound energy is not that sensitive. Moreover, the optical absorption edge of the strained silicane significantly shifts towards a low photon energy region and falls into the visible light range, which might serve as a promising candidate for optoelectronic devices. © 2014 AIP Publishing LLC. [<http://dx.doi.org/10.1063/1.4892110>]

## I. INTRODUCTION

As a stable and the thinnest two-dimensional (2D) honeycomb lattice in nature, graphene has attracted extensive attention and exhibits many unique properties like strong mechanical strength, exceptionally high carrier mobility, superior thermal conductivity, good transparency, and so on.<sup>1–6</sup> Interestingly, graphene itself is a zero-bandgap semimetal with Dirac-like electronic excitation,<sup>2,4</sup> while after full hydrogenation,<sup>7</sup>  $sp^2$  hybridized graphene is transformed into a buckled chair-like configuration with  $sp^3$  hybridized bonds (i.e., graphane)<sup>8–10</sup> that opens up a gap larger than 3.5 eV.<sup>11,12</sup> Clearly, both graphene and graphane lack a proper bandgap for most optoelectronic applications.

As a group IV element, when silicon (Si) atoms are arrayed in a hexagonal lattice, first-principles calculations reveal that the silicon nanosheet has a similar electronic structure as that of graphene.<sup>13–15</sup> Very recently, the monolayer silicon nanosheet, i.e., silicene, was synthesized into silver (111) and other (110) substrates.<sup>16–19</sup> Silicane (the analog of graphane) was also theoretically proposed,<sup>20–22</sup> with an appropriate bandgap of about 2.1 eV,<sup>21,23</sup> while the indirect bandgap might impede its potential application in optoelectronic devices.

Strain, as an effective means of tuning material properties, has been widely used to achieve controllable bandgaps in various 2D layered materials, like graphene, silicene, molybdenum disulfide ( $\text{MoS}_2$ ), etc. For example, the bandgap of graphene could be tuned in the order of 100 meV with a tensile strain.<sup>24</sup> Silicene would then, from a semimetal, become a metal under a tensile strain larger than 7.5%.<sup>25</sup> The application of a biaxial strain onto monolayer  $\text{MoS}_2$  would decrease the bandgap, and even induce a semiconductor-metal transi-

tion when the tensile strain is as large as about 8%.<sup>26</sup> Moreover, an experimental observation demonstrated that strain also has a great influence on the excitation energies in that compressive strain leads to higher energy while tensile strain induces lower energy for the same excitation in GaN epitaxial layers on sapphire and SiC substrates in comparison to strain-free bulk GaN.<sup>27</sup> In fact, many-body effects (e.g., electron-electron and electron-hole interactions) in low dimensional materials play a crucial role in electronic structures and optical absorption. In particular, excitonic effects (electron-hole interactions) can dramatically influence the position and intensity of the optical absorption spectra.<sup>28–31</sup> Therefore, it is highly desirable to include many-body effects for the study of the electronic and optical properties of silicane and their response to strain, for which there is no report so far.

In this work, we provide a systematic study of the electronic and optical responses of silicane to strain by using the density functional theory (DFT) in combination with many-body Green's function ( $GW$  approximation) and the Bethe-Salpeter equation (BSE) formalism. Our calculations show that silicane undergoes an indirect to direct bandgap transition under a small strain, and even a semiconductor to metal transition under a large strain. Furthermore, with the increase of tensile strain, a global red-shift of the absorption spectra is observed, and both the excitation energy of the lowest optically active exciton and the number of bright bound exciton states decrease.

## II. COMPUTATIONAL DETAILS

We first performed DFT calculations within the framework of local density approximation (LDA), implemented in QUANTUM ESPRESSO,<sup>32</sup> to obtain the electronic ground state of silicane with and without strain. A plane-wave basis

<sup>a)</sup>Electronic mail: jlwang@seu.edu.cn.

and norm-conserving pseudopotentials for ion-electron interactions were employed. The plane-wave cutoff energy was set to 60 Ry, and a Monkhorst-Pack mesh of  $18 \times 18 \times 1$  k-points was adopted. A vacuum region of 19 Å along the direction perpendicular to the silicane sheet was used to avoid interaction between two adjacent images. During geometry optimization, the cell parameters and atomic positions were fully relaxed until an energy convergence of less than  $10^{-4}$  eV was achieved and the force that acted on each atom was less than 0.02 eV/Å.

Starting from the electronic ground state wave functions, Coulomb screening, quasi-particle (QP) energies (single-particle excitation energies) can be obtained by solving Dyson's equation non-self-consistently within the  $G_0W_0$  approximation,<sup>33-36</sup>

$$\left[ -\frac{\nabla^2}{2} + V_{\text{ext}} + V_{\text{Hartree}} + \Sigma(E_{\text{nk}}^{\text{qp}}) \right] \psi_{\text{nk}}^{\text{qp}} = E_{\text{nk}}^{\text{qp}} \psi_{\text{nk}}^{\text{qp}}, \quad (1)$$

where  $V_{\text{ext}}$  is the ionic potential,  $V_{\text{Hartree}}$  is the Hartree potential,  $\Sigma$  is the self-energy operator,  $E_{\text{nk}}^{\text{qp}}$  is quasi-particle energies,  $\psi_{\text{nk}}^{\text{qp}}$  is the quasi-particle wavefunction. The self-energy operator  $\Sigma$  was calculated via the one-electron Green's function  $G_0$  and the dynamically screened Coulomb interaction  $W_0$ , i.e.,  $\Sigma = iG_0W_0$ . The dielectric matrix was evaluated by using random phase approximation (RPA)<sup>37</sup> and the frequency dependence of the self-energy operator was treated by using the Godby-Needs plasmon-pole approximation (PPA).<sup>38,39</sup> We also performed full-frequency  $GW$  calculation for unstrained silicane to benchmark the validity of PPA. An energy difference of only 0.01 eV was observed, which establishes the accuracy of PPA.

We further considered the excitonic effects by solving the Bethe-Salpeter equation which is a two-particle Green's function of the quasi-electron and quasi-hole states. This can be done through a diagonalization of the excitonic equation,<sup>36,40</sup>

$$(E_{\text{ck}}^{\text{qp}} - E_{\text{vk}}^{\text{qp}})A_{\text{vck}}^{\text{S}} + \sum_{k'v'c'} \langle \text{vck} | K^{\text{eh}} | v'c'k' \rangle A_{v'c'k}^{\text{S}} = \Omega_{\text{S}} A_{\text{vck}}^{\text{S}}, \quad (2)$$

where  $A_{\text{vck}}^{\text{S}}$  is the exciton amplitude,  $\Omega_{\text{S}}$  is the excitation energy,  $K^{\text{eh}}$  is the kernel that describes the interaction between excited electrons and holes;  $E_{\text{ck}}^{\text{qp}}$  and  $E_{\text{vk}}^{\text{qp}}$  are the quasi-particle energies of the electron and hole states;  $\langle \text{vck} |$  and  $| v'c'k' \rangle$  refer to the quasi-electron and quasi-hole states, respectively. The Bethe-Salpeter Hamiltonian was taken into account by using Tamm-Dancoff approximation (TDA),<sup>41</sup> in which the coupling term between the resonant and anti-resonant term of the Hamiltonian is neglected, and thus non-Hermitian BSE was reduced to that of Hermitian, and could be solved by using an efficient iterative method.<sup>42</sup> Finally, the macroscopic dielectric function can be expressed in terms of the eigenstates  $|\lambda\rangle$  and eigenvalues  $E_{\lambda}$  of Hamiltonian:<sup>35</sup>

$$\varepsilon_{\text{M}}(\omega) \equiv 1 - \lim_{q \rightarrow 0} \frac{8\pi}{|q|^2 \Omega N_{\text{q}}} \sum_{\text{nn}'k} \sum_{\text{mm}'k} \rho_{\text{nn}'k}^*(q, G) \rho_{\text{m}'\text{mk}}(q, G') \times \sum_{\lambda} \frac{A_{\text{nn}'k}^{\lambda} (A_{\text{m}'\text{mk}}^{\lambda})^*}{\omega - E_{\lambda}}, \quad (3)$$

where  $\Omega$  is the volume of unit cell,  $n$  ( $m$ ) and  $n'$  ( $m'$ ) are the band indices of the conduction and valence bands in

building the BSE kernel,  $k$  and  $k'$  are k-points on a uniform mesh grid in the first Brillouin zone.  $\rho_{\text{m}'\text{mk}}(q, G) = \langle m'k' | e^{i(q+G) \cdot r} | mk' - q \rangle$ ,  $G$  are the reciprocal lattice vectors, and  $A_{\text{nn}'k}^{\lambda} = \langle n'nk | \lambda \rangle$  are the eigenvectors of Hamiltonian.

In both the  $GW$  and BSE calculations, screened coulomb interaction was truncated after 20 a.u. along the direction perpendicular to the surface in order to avoid spurious interaction between periodic images. 360 (384) unoccupied bands, 12 Ry and 49.6 Ry energy cutoff are adopted to obtain the dielectric matrices and exchange energy; and 5 valence bands and 15 unoccupied bands are taken to achieve the optical absorption spectra for silicane with and without strain, respectively. A  $k$ -point sampling of  $18 \times 18 \times 1$  is used during the  $GW$  calculation and we interpolate to  $24 \times 24 \times 1$  k-point sampling for BSE calculation. These parameters are all converged within 0.05 eV for  $GW$  gap and absorption spectra. The  $GW$  and BSE calculations were performed by using the YAMBO program package.<sup>35</sup>

### III. RESULTS AND DISCUSSION

Previous studies have shown that silicane with a chair-like configuration is the most stable structure among the hydrogen decorated silicene,<sup>43,44</sup> so we took this structure as the computational model in our work. The optimized structure is shown in Figure 1(a) with a lattice constant of 3.82 Å, which is in good agreement with a previous result of 3.82 Å.<sup>20</sup> The Si-Si bond length is 2.32 Å, which has also reproduced well the previous experimental value of 2.35 Å.<sup>45</sup> The buckling parameter  $\Delta$  (height difference between two adjacent Si atoms) is 0.71 Å and the Si-H bond length is about 1.50 Å, which are consistent with earlier reports as well.<sup>18,21</sup> In this study, a uniform biaxial tensile strain was applied along the zigzag (vertical direction in Figure 1(a)) and armchair directions (horizontal direction in Figure 1(a)) simultaneously. In applying the biaxial tensile strain from  $\delta = 0\%$  to 22%, the buckling height in the silicane decreases from 0.71 to 0.51 Å

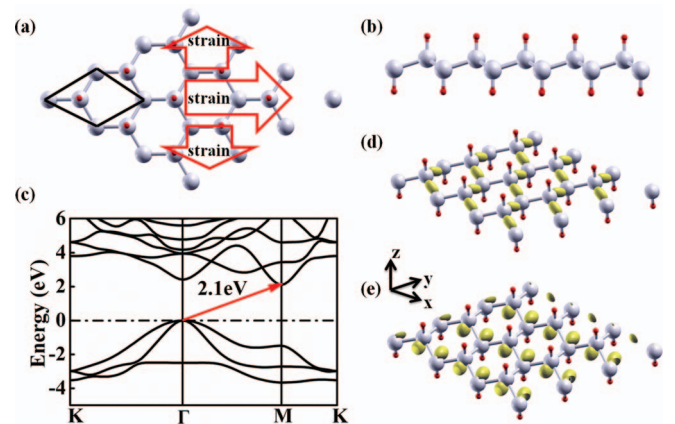


FIG. 1. (a) Top and (b) side views of optimized silicane with a chair-like configuration. The black rhombus represents the primitive cell; white (large) and red (small) spheres represent silicon and hydrogen atoms, respectively. (c) Band structure. The VBM is shifted to zero; the solid red arrow indicates the indirect bandgap. (d) and (e) partial charge density of VBM and CBM, respectively.

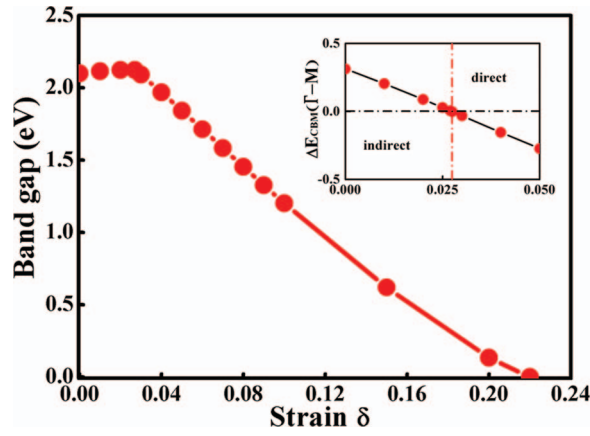


FIG. 2. Bandgap as a function of strain for silicane. Insert shows energy difference between  $\Gamma$ -CBM and M-CBM vs. strain.

and the Si-Si bond length is elongated from 2.32 to 2.74 Å, while the Si-H bond lengths are almost the same.

### A. Electronic band structure

Silicane is an indirect wide bandgap semiconductor, with a valence band maximum (VBM) located at  $\Gamma$ -point ( $\Gamma$ -VBM) and the conduction band minimum (CBM) at the M-point (M-CBM), as shown in Figure 1(c). The calculated LDA bandgap is 2.1 eV, which is in good agreement with previous results.<sup>20,21</sup> Both the VBM and CBM states of silicane originate from the contribution of the Si-3*p* states, as can be seen from the partial charge density in Figures 1(d) and 1(e). The CBM is composed of the  $\sigma^*$  anti-bonding states of the Si-Si bonds along the x-y plane, while the VBM is composed of the  $\sigma$  bonding states of the Si-Si bonds along the zigzag lines. Under a uniform tensile strain, the bandgap slightly increases first and reaches the maximum value at about  $\delta = 2.74\%$  and then rapidly decreases with increase of strain, and the gap is reduced by about 43% at  $\delta = 10\%$  compared to that without strain (see Figure 2). This can be understood as follows. When tensile strain is applied, the Si-Si bond length increases as shown in Table I and the Si-Si bond strength decreases accordingly. As a result, the  $\Gamma$ -CBM greatly shifts downward, thus leading to the eventual decrease of the bandgap. Moreover, when  $\delta$  reaches 22%, the CBM and VBM of silicane coincide at the  $\Gamma$  point, which suggests a semiconductor to metal transition. Accompanied with the variation of the gap values, the band structures of silicane change under strain as

TABLE I. Structural parameters of silicane with and without strain: strain ( $\delta$ ), lattice constant (*a*; Å), bond length ( $d_{\text{Si-Si}}$ ; Å), and buckling height ( $\Delta$ ; Å). The electron affinity (EA; eV), Löwdin charge (C; e) transferred from Si to H atoms, excitation energy ( $E_e$ ; eV), and bound energy ( $E_b$ ; eV) of the lowest optically active exciton.

$\delta$	<i>a</i>	$d_{\text{Si-Si}}$	$\Delta$	$E_{g\text{-LDA}}$	$E_{g\text{-GW}}$	EA	C	$E_e$	$E_b$
0.00	3.82	2.32	0.71	2.10	4.15	2.30	0.181	3.22	0.93
0.03	3.94	2.37	0.67	2.09	3.76	2.83	0.190	2.86	0.90
0.06	4.05	2.42	0.63	1.71	3.28	3.52	0.199	2.42	0.86
0.10	4.20	2.50	0.59	1.20	2.58	4.18	0.210	1.82	0.76

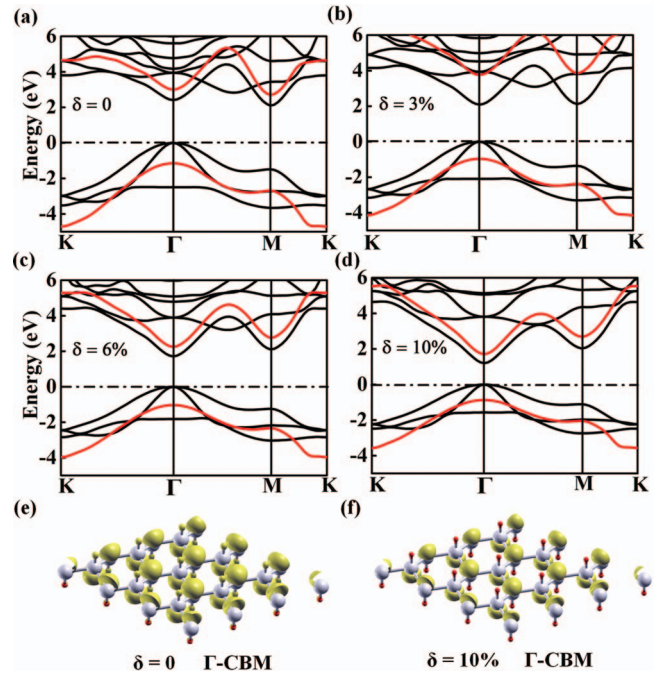


FIG. 3. (a)–(d): Band structures of silicane at  $\delta = 0, 3, 6,$  and  $10\%$  from LDA calculations (black solid lines) and the red solid lines represent QP energies corrections to the LDA energies at relevant k-points of the uppermost valence band and the lowest conduction band in the  $G_0W_0$  approximation. Partial charge density of the conduction band minimum at the  $\Gamma$  point ( $\Gamma$ -CBM) without strain (e) and with strain  $\delta = 10\%$  (f), respectively.

well as reflected in Figures 3(a) to 3(d). The tensile strain reduces the energy gap between  $\Gamma$ -CBM and M-CBM in the range of  $\delta = 0\% - 2.74\%$  (see Figure 2) and an indirect to direct bandgap transition occurs at  $\delta = 2.74\%$ . Moreover, the CBM moves to the  $\Gamma$  point and the silicane becomes a direct bandgap semiconductor under a broad strain range of  $2.74\% < \delta < 22\%$ .

To understand why the energy of  $\Gamma$ -CBM is essentially affected by the strain in silicane, we calculated the partial charge density at the  $\Gamma$ -point for CBM which is shown in Figures 3(e) and 3(f). In the strain-free case, the charge density of  $\Gamma$ -CBM shows a  $\sigma^*$  bond-like feature and is primarily located around the Si and H atoms. Nevertheless, when the strain reaches the value of 10%, the charge density is redistributed to one side (top or bottom of Si atoms). Thus, the interaction between the hybridized *s-p* orbitals ( $\sigma^*$  bonds) is weakened, which results in the downward shift of  $\Gamma$ -CBM.

At the DFT-LDA level, silicane is a semiconductor with an indirect bandgap of 2.1 eV. However, it is well-known that the standard Kohn-Sham DFT generally underestimates the bandgap. When electron-electron self-energy effects are included, the opening of the bandgaps is found to be sizable (more than 50% compared to the LDA gaps in our calculations). Nevertheless, their semiconducting nature does not change, that is, the QP band structure of silicane is also indirect for strain  $\delta = 0$  and direct for  $\delta \geq 2.74\%$ . The QP bandgap of silicane without strain is 4.15 eV, in accordance with the previous result of 4.07 eV.<sup>23</sup> Moreover, the QP bandgaps of silicane rapidly decrease from 4.15 to 2.58 eV as the strain increases from  $\delta = 0\%$  to  $\delta = 10\%$  (see Table I). Generally, the

many-body effects will be enhanced in the atomic-layer systems due to the low dimensionality, which has been observed in graphane<sup>46</sup> and MoS<sub>2</sub>.<sup>47,48</sup> Moreover, the many-body effects can significantly modify electron affinity and ionization potential, which can be determined from the accurate measuring of the CBM and VBM with respect to the vacuum level (Figures 3(a)–3(d)), respectively. For silicane, we identified a dramatic change of the electron affinity from 2.30 eV ( $\delta = 0$ ) to 4.18 eV ( $\delta = 10\%$ ). The increased electron affinity with increase of strain suggests that more charge transfers from Si atoms to H atoms, as shown in Table I. This fact has direct influence on the transition from an indirect to a direct bandgap and the decrease of the bandgap.

## B. Optical properties

Figure 4(a) presents the optical absorption spectra of silicane for light polarization parallel to the surface plane. The plotted quantity “ $\text{Im } \epsilon_M$ ” is the imaginary part of the macroscopic dielectric function from (3). Compared with the independent-particle results, there is evident weight redistribution of the oscillator strength in the optical absorption spectra which includes self-energy effects and electron-hole interactions, thus showing a global red-shift of the whole spectrum due to the excitonic effects. Below the continuum onset of single-particle transition, there are strongly bound

excitons. Additionally, with the increase of strain, a number of bound exciton states with different oscillator strengths below the fundamental QP gap are observed, which shift the absorption edge from the ultraviolet to the visible spectral range. Meanwhile, the e-h interaction and the electron/hole effective masses have great impacts on the number of bright bound exciton states, e.g., stronger e-h interactions or large electron (holes) effective masses mean more bright bound excitons. Besides that, there is an obvious decrease in the bandgap opening due to self-energy effects, as shown in Table I. For silicane, the excitation energy of the lowest optically active (bright) exciton  $A^1$  is 3.22 eV, with a bound energy of 0.93 eV, which agrees with the previous result of 0.9 eV.<sup>12</sup> Vertical transitions from the top of the valence band to the bottom of the conduction band close to the  $\Gamma$ -point contribute to strongly bound excitons ( $A^1$ ).  $A^1$  is also degenerated with a dark exciton with much smaller oscillator strength. In the case of strained silicane, the bound energies of the lowest bound excitons are 0.93, 0.90, 0.86, and 0.76 eV for  $\delta = 0, 3\%, 6\%$ , and  $10\%$ , respectively (see Table I). By analyzing these excitonic bound states, we find that the main contributions are still from the transitions between the last valence and first conduction bands close to the  $\Gamma$ -point. Therefore, all of these excitons aforementioned are twofold degenerate.

To gain further insight on the optical spectra, we calculated the electron probability distribution that is related to

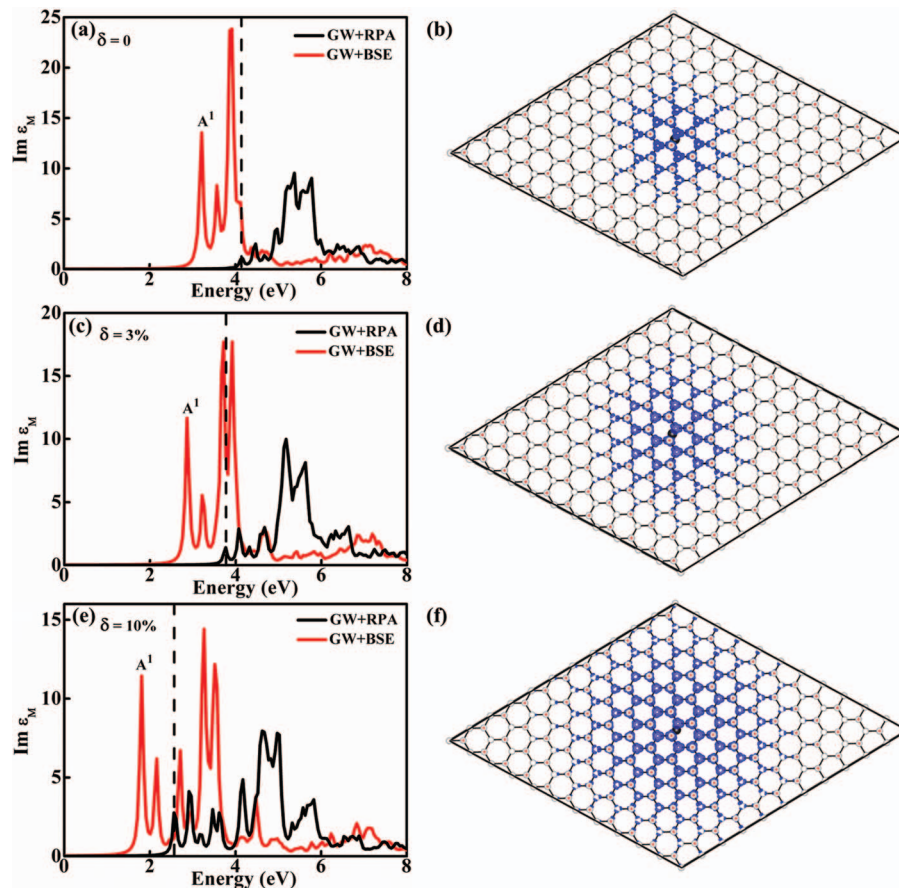


FIG. 4. (a), (c), and (e): optical absorption spectra of silicane ( $\delta = 0, 3\%, 10\%$ ) with and without e-h interaction, i.e.,  $GW+BSE$  and  $GW+RPA$ , respectively.  $A^1$  denotes the first bright bound exciton. The vertical black dashed lines indicate the lowest direct QP gap. (b), (d), and (f): top view of the lowest energy exciton ( $A^1$ ) wave function in silicane ( $\delta = 0, 3\%, 10\%$ ) with the hole position (black dot) fixed on Si-Si bond.

the main peaks of the absorption spectra. The excitonic wave function can be written as

$$|\psi^S(r_e, r_h)\rangle = \sum_{cvk} A_{cvk}^S \psi_{ck}(r_e) \psi_{vk}^*(r_h), \quad (4)$$

where  $r_e$  and  $r_h$  are the electrons and hole coordinates in real space, respectively.  $\Psi$  is the quasi-particle wavefunction. The coefficient  $A_{cvk}^S$  is obtained by diagonalizing the Hamiltonian of the Bethe-Salpeter equation. To represent the six coordinate function, we fixed the hole position on the Si-Si bond and projected the electron probability  $|\Psi^S[r_e, r_h = (0, 0, 0)]|^2$  onto the  $x$ - $y$  plane. Figures 4(b), 4(d), and 4(f) show the electron probability distribution for the bound exciton ( $A^1$ ) of silicane and strained silicane, and on two sub-lattices, which reflects the bound strength between the excited electron and the hole. As clearly seen from Figure 4(b), the exciton spreads in a relatively localized space with an exciton radius of 12 Å for silicane, thus suggesting a relatively large bound energy. However, the exciton radius is 15 Å and 21 Å for  $\delta = 3\%$  and 10%, respectively, indicating that the applied strain can increase the exciton radius. In a previous theoretical study,<sup>44</sup> graphane was considered as a potential candidate for excitonic Bose-Einstein condensation (BEC) due to the extremely large bound energy and strong localization of the bound excitons. However, realization of BEC in silicane and strained silicane seems to be less feasible since their exciton bound energies are not as large as that of graphane together with a relatively large exciton radius.

#### IV. CONCLUSIONS

In summary, we have studied the electronic structure and optical properties of silicane under uniform biaxial tensile strain by using the DFT and *GW*-BSE calculations. An indirect to direct bandgap transition can be achieved when the applied strain is about 2.74%. The semiconducting silicane can even be tuned into a metal under an extremely large strain of 22%. The bandgap transitions are attributed to the downward shift of the lowest conduction band at the  $\Gamma$ -point as the strain increases, which weakens the  $\sigma^*$  bond and thereby increases the electron affinity of silicane significantly. Due to the rather weak screening and low dimensionality effects, the QP bandgaps of silicane are 4.15, 3.76, 3.28, and 2.58 eV, and the bound energies of the lowest bound excitons are 0.93, 0.90, 0.86, and 0.76 eV for  $\delta = 0, 3\%, 6\%$ , and 10%, respectively. The optical absorption edge of strained silicane shifts towards a low photon energy region and falls into the visible light range, which makes it a compelling candidate for optoelectronic devices. The large bound energies and oscillator strengths of the lowest excitons, together with their 2D feature, suggest that interesting physical effects can be observed as well.

#### ACKNOWLEDGMENTS

This work is supported by the NBRP (2010CB923401, 2011CB302004), NSF (21173040, 21373045), and of Jiangsu (BK20130016) and SRFDP (20130092110029) in China. The

authors thank the computational resources at the SEU and the National Supercomputing Center in Tianjin.

- <sup>1</sup>A. K. Geim, *Science* **324**, 1530 (2009).
- <sup>2</sup>A. H. Castro Neto, F. N. Guinea, M. R. Peres, K. S. Novoselov, and A. K. Geim, *Rev. Mod. Phys.* **81**, 109 (2009).
- <sup>3</sup>T. J. Shao, B. Wen, R. Melnik, S. Yao, Y. Kawazoe, and Y. Tian, *J. Chem. Phys.* **137**, 194901 (2012).
- <sup>4</sup>D. S. L. Abergel, V. Apalkov, J. Berashevich, K. Ziegler, and T. Chakraborty, *Adv. Phys.* **59**, 261 (2010).
- <sup>5</sup>C. Lee, X. Wei, W. Kysar, and J. Hone, *Science* **321**, 385 (2008).
- <sup>6</sup>L. Y. Zhu, J. L. Wang, T. T. Zhang Ma, C. W. L. Lim, F. Ding, and X. C. Zeng, *Nano Lett.* **10**, 494 (2010).
- <sup>7</sup>D. C. Elias, R. R. Nair, T. M. G. Mohiuddin, P. Black, M. P. Halsall, A. C. Ferrari, D. W. Boukhvalov, M. I. Katsnelson, A. K. Geim, and K. S. Novoselov, *Science* **323**, 610 (2009).
- <sup>8</sup>J. O. Sofo, A. S. Chaudhari, and G. D. Barber, *Phys. Rev. B* **75**, 153401 (2007).
- <sup>9</sup>O. Leenaerts, H. Peelaers, A. D. Hernandez-Nieves, B. Partoens, and F. M. Peeters, *Phys. Rev. B* **82**, 195436 (2010).
- <sup>10</sup>L. Y. Zhu, H. Hu, Q. Chen, S. D. Wang, J. L. Wang, and F. Ding, *Nanotechnology* **22**, 185202 (2011).
- <sup>11</sup>F. Karlický, R. Zbořil, and M. Otyepka, *J. Chem. Phys.* **137**, 034709 (2012).
- <sup>12</sup>O. Pulci, P. Gori, M. Marsili, V. Garbuio, R. Del Sole, and F. Bechstedt, *Europhys. Lett.* **98**, 37004 (2012).
- <sup>13</sup>S. Cahangirov, M. Topsakal, E. Akturk, H. Sahin, and S. Ciraci, *Phys. Rev. Lett.* **102**, 236804 (2009).
- <sup>14</sup>Y. Ding and J. Ni, *Appl. Phys. Lett.* **95**, 083115 (2009).
- <sup>15</sup>S. D. Wang, L. Y. Zhu, Q. Chen, J. L. Wang, and F. Ding, *J. Appl. Phys.* **109**, 053516 (2011).
- <sup>16</sup>C. Leandri, G. Le Lay, B. Aufray, C. Girardeaux, J. Avila, M. E. Davila, M. C. Asensio, C. Ottaviani, and A. Cricenti, *Surf. Sci.* **574**, L9 (2005).
- <sup>17</sup>G. Le Lay, B. Aufray, C. Landri, H. Oughaddou, J. P. Biberian, P. De Padova, M. E. Dvila, B. Ealet, and A. Kara, *Appl. Surf. Sci.* **256**, 524 (2009).
- <sup>18</sup>B. Aufray, A. Vizzini, S. Oughaddou, H. Leandri, C. Ealet, and G. Le Lay, *Appl. Phys. Lett.* **96**, 183102 (2010).
- <sup>19</sup>B. Lalmi, H. Oughaddou, H. Enriquez, A. Kara, S. Vizzini, B. Ealet, and B. Aufray, *Appl. Phys. Lett.* **97**, 223109 (2010).
- <sup>20</sup>L. C. Lew Yan Voon, E. Sandberg, R. S. Aga, and A. A. Farajian, *Appl. Phys. Lett.* **97**, 163114 (2010).
- <sup>21</sup>M. Houssa, E. Scalise, K. Sankaran, G. Pourtois, V. V. Afanasev, and A. Stesmans, *Appl. Phys. Lett.* **98**, 223107 (2011).
- <sup>22</sup>J. C. Garcia, D. B. de Lima, L. V. C. Assali, and J. F. Justo, *J. Phys. Chem. C* **115**, 13242 (2011).
- <sup>23</sup>W. Wei and T. Jacob, *Phys. Rev. B* **88**, 045203 (2013).
- <sup>24</sup>G. Gui, J. Li, and J. Zhong, *Phys. Rev. B* **78**, 075435 (2008).
- <sup>25</sup>G. Liu, M. S. Wu, C. Y. Ouyang, and B. Xu, *Europhys. Lett.* **99**, 17010 (2012).
- <sup>26</sup>E. Scalise, M. Houssa, G. Pourtois, V. Afanas'ev, and A. Stesmans, *Nano Res.* **5**(1), 43 (2012).
- <sup>27</sup>W. Shan, R. J. Hauenstein, A. J. Fischer, J. J. Song, W. G. Perry, M. D. Bremser, R. F. Davis, and B. Goldenberg, *Phys. Rev. B* **54**, 13460 (1996).
- <sup>28</sup>S. D. Wang and J. L. Wang, *J. Phys. Chem. C* **116**, 10193 (2012).
- <sup>29</sup>S. D. Wang, Q. Chen, and J. L. Wang, *Appl. Phys. Lett.* **99**, 063114 (2011).
- <sup>30</sup>L. Yang, *Phys. Rev. B* **83**, 085405 (2011).
- <sup>31</sup>B. Arnaud, S. Lebègue, P. Rabiller, and M. Alouani, *Phys. Rev. Lett.* **96**, 026402 (2006).
- <sup>32</sup>P. Giannozzi *et al.*, *J. Phys.: Condens. Matter* **21**, 395502 (2009).
- <sup>33</sup>L. Hedin, *Phys. Rev.* **139**, A796 (1965).
- <sup>34</sup>L. Hedin and S. Lundqvist, *Solid State Physics* **23**, 1 (1970).
- <sup>35</sup>A. Marini, C. Hogan, M. Grüning, and D. Varsano, *Comput. Phys. Commun.* **180**, 1392 (2009).
- <sup>36</sup>M. Rohlfing and S. G. Louie, *Phys. Rev. B* **62**, 4927 (2000).
- <sup>37</sup>R. Ahuja, S. Auluck, J. M. Wills, M. Alouani, B. Johansson, and O. Eriksson, *Phys. Rev. B* **55**, 4999 (1997).
- <sup>38</sup>R. W. Godby and R. J. Needs, *Phys. Rev. Lett.* **62**, 1169 (1989).
- <sup>39</sup>A. Oschlies, R. W. Godby, and R. J. Needs, *Phys. Rev. B* **51**, 1527 (1995).
- <sup>40</sup>E. E. Salpeter and H. A. Bethe, *Phys. Rev.* **84**, 1232 (1951).
- <sup>41</sup>A. L. Fetter and J. D. Walecka, *Quantum Theory of Many-Particle Systems* (Dover, New York, 2003), Chap. 15, p. 565.

- <sup>42</sup>M. Gruning, A. Marini, and X. Gonze, *Nano Lett.* **9**, 2820 (2009).
- <sup>43</sup>Y. Ding and Y. Wang, *Appl. Phys. Lett.* **100**, 083102 (2012).
- <sup>44</sup>P. Zhang, X. D. Li, C. H. Hu, S. Q. Wu, and Z. Z. Zhu, *Phys. Lett. A* **376**, 1230 (2012).
- <sup>45</sup>J. R. Dahn, B. M. Way, and E. Fuller, *Phys. Rev. B* **48**, 17872 (1993).
- <sup>46</sup>P. Cudazzo, C. Attaccalite, L. V. Tokally, and A. Rubio, *Phys. Rev. Lett.* **104**, 226804 (2010).
- <sup>47</sup>K. F. Mak, C. Lee, J. Hone, J. Shan, and T. F. Heinz, *Phys. Rev. Lett.* **105**, 136805 (2010).
- <sup>48</sup>A. Molina-Sánchez, D. Sangalli, K. Hummer, A. Marini, and L. Wirtz, *Phys. Rev. B* **88**, 045412 (2013).